

DELIVERABLE 8

*Deliverable 8: Measurement protocols
for dimensional characterisation of
microfluidic components*

(A4.3.3)

Work package 4

Organisation Name of Lead Partner for D8: RISE

Submission Date: 27 April 2024



The EMPIR initiative is co-funded by the European Union's Horizon 2020 research and innovation programme and the EMPIR Participating States

<https://mfmet.eu>

This report was written as part of activity A4.3.3 from the EMPIR Establishing Metrology Standards in Microfluidic Devices (MFMET) project. The three-year European project commenced on 1st June 2021 and focused on providing a generic methodology of accurate measurement of a particular quantity in a microfluidic device by utilising standardised methods and reference documents, e.g. VIM & GUM. For more details about this project, please visit <https://mfmet.eu>.

This report was written by:

Name	Institution	E-mail
Oliver Büker	RISE	oliver.buker@ri.se
Christina Pecnik	IMT AG	cpecnik@imtag.ch
Elena Müller	microfluidic ChipShop	elena.mueller@microfluidic-chipshop.com
Henne van Herren	EnablingMNT	henne@enablingmnt.com
Vania Silverio	INESC MN	vsilverio@inesc-mn.pt
Nicolas Feltin	LNE	nicolas.feltin@lne.fr
Joris Kaal	CEA	joris.kaal@cea.fr
Elsa Batista	IPQ	ebatista@ipq.pt

EMPIR



The EMPIR initiative is co-funded by the European Union's Horizon 2020 research and innovation programme and the EMPIR Participating States

Contents

1	Scope.....	3
2	Materials in microfluidics.....	3
2.1	Polymers	3
2.2	Glass	4
3	Dimensional characterisation of microfluid components	4
3.1	Optical microscopy.....	4
3.2	White light interferometer	5
3.3	Confocal laser (scanning) microscopy.....	5
3.4	Profilometer	5
3.5	Atomic force microscopy (AFM)	6
4	Dimensional parameters and measurement methods.....	7
4.1	Polymers	7
4.2	Glass	8
5	Example protocols for measuring the dimensional characteristics of transfer standards	9
5.1	Glass transfer standards	9
5.2	Instruments.....	9
5.3	Measurements procedure using a binocular microscope	11
5.4	Image tiling to measure a whole device	13
5.4.1	Procedure of tiling	13
5.5	Height measurements using confocal microscopy	14
5.6	Measurements procedure using an optical profilometer.....	17
5.7	Conclusions	18
6	References	18
	ANNEX (Appendix) 1	19

1 Scope

This document provides measurement protocols for dimensional properties, accuracy determination and measurements of microfluidic components.

The measurement protocols serve as a guide for NMI/DI planning to introduce new calibration services, such as the internal dimensions of channels (diameter/length/width).

Finally, the protocol includes an example where the glass transfer standards produced in A2.4.2 have been tested according to this document.

Activity number	Activity description	Partners (Lead in bold)
A3.3.3 M33	<p>Using input from A4.3.1 and A4.3.2, RISE with support from IMTAG, microfluidic, BHT and LNE will define by April 2023 (M23) measurement protocols for dimension characteristics, accuracy determination and measurements of microfluidic components.</p> <p>The measurement protocols will be used for building the transfer standards in A2.4.2. The protocols will be used also for testing the transfer standards once they are built, and this testing will in turn lead to updating the protocols by February 2024 (M33).</p> <p>Once agreed by the consortium, the coordinator on behalf of RISE, IMTAG, microfluidic, BHT and LNE will submit the measurement protocols to EURAMET as D8: '<i>Measurement protocols for dimensional characterisation of microfluidic components</i>'.</p> <p>These measurement protocols will be used as guidelines for NMI/DIs wishing to introduce new calibration services such as inner dimensions of channels (diameter/length/width).</p>	RISE , IMTAG, LNE, microfluidic, BHT

2 Materials in microfluidics

The reliability of microfluidic devices is determined by the interaction of all the materials involved. The choice of materials depends mainly on the specific use and function of the final microfluidic device, but the availability of manufacturing technology and production costs can also play an important role.

In general, the three most important material groups for microfluidics can be defined:

- Polymers
- Inorganic materials (glass, silicon, oxides)
- Metals

In this report, the focus is on two widely used materials: polymers and glass.

2.1 Polymers

There are three main classes of polymers or plastics:

Thermosetting

Thermosetting polymers have a high capacity to resist higher temperature and retain their strength and shape when heated. They have a little bit of flexibility and are impermeable. They cannot be molded more than once. For instance: epoxies.

Thermoplastics

Thermoplastic polymers have good creep resistance and are electrically insulated. They can be melted and solidified many times. Examples: PMMA (polymethyl methacrylate), PEEK (polyether ether ketone), PP (polypropylene), PS (polystyrene), PTFE (polytetrafluoroethylene), FEP (fluorinated ethylene propylene), PC (polycarbonate), COC (cyclic olefin copolymer)/COP (cyclic olefin polymers).

Elastomers

Elastomers are flexible and have a low creep resistance. There are two types:

- a) Thermoplastic elastomers (can be melted)
- b) Thermoset elastomers (cannot be melted)

Examples of elastomers/synthetic rubber: EPDM (ethylene propylene diene rubber), FFKM (perfluorinated elastomer) and silicone.

2.2 Glass

The most commonly used glass types for microfluidic components are D236® T eco, D236® bio and MEMpax® (all 3 from SCHOTT). Their properties are described in the suppliers' data sheets, which are available online or can be obtained directly from the supplier on request.

The material properties relevant to the selection of the base material prior to processing into microfluidic parts and components are listed in Table 1.

In general, all three glass types are suitable for microfluidic applications, but their use may vary depending on specific requirements. D236® bio exhibits very low intrinsic autofluorescence across the UV to NIR spectrum compared to D236® T eco. In addition, spectral transmittance provides information on the optical properties of the substrate, such as optical density, reflectance or transparency.

When glass is combined with silicon, MEMpax® should be selected to avoid stresses caused by thermal expansion (CTE of silicon $\sim 2.6 \mu\text{K}$). In the worst case, such induced stresses can lead to breakage of the entire component.

3 Dimensional characterisation of microfluid components

There are various measurement methods available for measuring the diameter, length and width of microfluid components, e.g. microfluidic channels. Geometrical dimensions relevant for microfluidic components are defined in ISO 22916:2021(E).

The most important methods: optical microscopy, white light interferometer, confocal laser microscopy, profilometer, AFM (see also chapter 4) are briefly presented below.

3.1 Optical microscopy

Optical microscopes are microscopes that produce highly magnified images of small structures or objects using light. Magnification takes place according to the laws of optics by utilising light refraction on glass lenses. In order to recognise structures in the generated image, the image must contain sufficient contrast. The most common microscopic technique for such objects is bright-field microscopy, in which contrast is created by coloured or dark structures in the illuminated specimen, if necessary enhanced by additional artificial colouring of the object. In colourless specimens, contrast can also be created using special illumination methods by converting differences in optical density into differences in brightness. Examples of this are dark-field microscopy, phase-contrast microscopy and differential interference contrast microscopy. Differences in the polarisation behaviour of the

specimen are used in petrographic microscopy. For fluorescence microscopy and its numerous special procedures, fluorescent structures in the specimen are a prerequisite. Other microscopic methods include confocal microscopy, in which, in contrast to conventional light microscopy, only a fraction of the specimen is illuminated at any one time rather than the entire specimen, and two-photon excitation microscopy, which works in a similar way to confocal laser scanning microscopy.

3.2 White light interferometer

High precision white light interferometers are used for non-contact distance and thickness measurements. White light interferometers enable stable measurement results with sub-nanometre resolution and offer a comparatively large measurement range and offset distance.

White light interferometers use infrared light in the invisible range (wavelength about 840 nm), which means that the measurement position is not visible. To visualise the measurement position, most systems are equipped with a pilot laser that projects a point of light onto the measurement position. If the measurement object is at the correct distance and within the measurement range, a constant light is emitted by the pilot laser. If the measurement object is outside the measurement range, the pilot laser flashes.

The industrial white light interferometer consists of a robust sensor, a highly flexible sensor cable and a control unit in an aluminium housing that can be mounted on a DIN (Deutsches Institut für Normung) rail. The controller has an active temperature control that compensates for changes in ambient temperature and thus achieves enormous temperature stability. Thanks to its robust design, the interferometer can also be integrated into industrial environments. Cable lengths of up to 10 metres also enable spatial separation of sensor and controller. For cleanroom and vacuum measurement tasks, vacuum-adapted sensors, cables and cable entry accessories are available.

3.3 Confocal laser (scanning) microscopy

A confocal microscope is a special type of light microscope. In contrast to conventional light microscopy, the entire specimen is not illuminated, but only a part of it at any one time, in many cases only a small spot of light.

The specimen is rasterised piece by piece. The microscope therefore never captures a complete image. The light intensities of the reflected light or light emitted by fluorescence are therefore measured successively at all locations of the area, so that a subsequent construction of the image is possible.

A pinhole diaphragm is fitted in the beam path of the detected light, which only allows light from the focussed area to pass through and blocks light from other planes. As a result, only light around the focal point reaches the detector, so that optical sectional images with high contrast are generated.

Confocal microscopes are available in many different designs. Point scanners in which a focussed laser beam scans the specimen are widely used (confocal laser scanning microscope, CLSM).

With line scanners, on the other hand, an entire image line is created at once so that a higher speed can be achieved. A third variant uses a so-called Nipkow disc, on which several pinholes are arranged in a spiral. As the disc rotates, each pinhole scans a circular curve of the specimen. This variant also uses either white light or fluorescence. The latter is referred to as a fluorescence microscope.

3.4 Profilometer

A profilometer is a measuring instrument for quantifying the roughness of a surface. The vertical resolution is usually the nanometre while the lateral resolution is usually lower. A profilometer is a measuring device for the two- or three-dimensional measurement of microscopic or sub-microscopic surface topographies. Profilometers work either tactilely, using a small diamond needle (stylus) to scan the surface, or non-contact, using optical methods such as confocal technology, laser profilometry or white light interferometry. The diamond needle is moved vertically into contact with the sample and then laterally across the sample to measure specific contact distances and forces. A

profilometer can measure small surface deviations in the vertical direction as a function of stylus position. A typical profilometer can measure differences in the order of 10 nm to 1 mm. The height position of the diamond stylus generates an analogue signal which is converted to a digital signal, analysed and transmitted to the display. The radius of the diamond stylus is in the range of 20 nm to 25 μm and the horizontal resolution is controlled by the scanning and scanning speed of the signal. The force exerted by the stylus is often in the range of less than 1 to 50 milligram-force (0.01 mN to 1 mN). Most surface precision standards in the world are realised with contact profilometers. In many cases, contact with the surface is an advantage in the case of contaminated samples, where non-contact methods can deliver incorrect results. The contact method, as a direct technique, is not based on the reflectance or colour of the surface.

An optical profilometer is a non-contact method and can provide similar information compared to a tactile (contact) profilometer. There are many different techniques currently available, such as laser triangulation, confocal microscopy (for profiling very small objects) and digital holography. Optical profilometers can work very fast, as the surface is not touched, the scanning speed depends only on the speed of light reflection on the surface and the detection speed of the device electronics. As optical profilometers do not touch the surface, no damage can occur. Many non-contact profilers also require little maintenance. Due to the small beam size, the lateral resolution ranges from a few micrometres to less than one micrometre.

3.5 Atomic force microscopy (AFM)

The atomic force microscope, also known as atomic/scanning force microscope (abbreviations AFM or SFM, more rarely RKM), is a special scanning probe microscope. It is an important technique in surface measurement and is used for the mechanical scanning of surfaces and the measurement of atomic forces in the nanometre range. A nanoscopically fine needle is pressed against the sample to be measured by means of a leaf spring (cantilever), and the atomic forces bend the cantilever. This deflection can be measured with light and the force acting between the atoms on the surface and the tip can be calculated. Since no electrical current flows between the sample and the tip, non-conductive samples can also be analysed. By recording the deflections or forces point by point, an image of the sample surface can be generated in the same way as a digital photo. Each individual pixel then represents a specific measured value. As with profilometers, the possible resolution of the image is mainly determined by the radius of curvature of the tips, which is usually 10 nm to 20 nm, allowing lateral resolutions of 0.1 nm to 10 nm depending on the roughness of the sample surface. This is sufficient to even image individual atoms in the ideal case. Together with the scanning tunnelling microscope (STM), the atomic force microscope therefore has the highest resolution of all microscopic techniques.

4 Dimensional parameters and measurement methods

4.1 Polymers

The most commonly used method for manufacturing microfluidic devices from thermoplastic polymers is injection moulding, as it is highly reproducible, precise and cost-effective for industrial mass production. The dimensions of the chips are controlled during the manufacturing process.

Table 1 – Properties and their characterisation for polymer types.

Material property	Reference standard	Measured value		
		mcs-COP 02	mcs-COC 13	mcs-PC 13
Thickness tolerance	ISO 22081	$\pm \dots \mu\text{m}^*$		
Total thickness variation (TTV)	ISO 22081	$\leq \dots \mu\text{m}^*$		
Flatness	ISO 22081	$\leq \dots \mu\text{m}^*$		
Linear expansion coefficient	ISO 11359-1/-2	70 [$\mu\text{m}/\text{K}$]	60 [$\mu\text{m}/\text{K}$]	65 [$\mu\text{m}/\text{K}$]

*Depends on substrate thickness

As in the case of polymer chips, the smooth surface of the microfluidic channels is crucial for the flow behaviour in the microfluidic channels. During the manufacturing process, the surface can be treated differently to make it more hydrophilic or hydrophobic, for example, depending on the intended application.

In summary, Table 2 shows the physical parameters of the polymers that are relevant for microfluidic components manufacturer and describes the measurement techniques that can be used to characterise the relevant dimensional measurement quantity in polymer microfluidic component.

Table 2 – Dimensional measured quantities and their measurement technology that are relevant for plastic parts during and after processing microfluidic components.

Dimensional measured quantities in/on polymers microfluidic components	Method	Measured value
Channel dimensions like depth or width	Optical microscope; confocal laser microscopy, profilometer	dimension [μm]
Dimensions of coating structures	Optical microscope; confocal laser microscopy, profilometer	dimension [μm]
Surface roughness of the channel, coating or device surface	Confocal laser microscopy; ISO 4287	R_a value [nm] = arithmetic mean height

4.2 Glass

To convert a glass substrate into a microfluidic part/device, processes similar to those used in the semiconductor industry are applied. The dimensional properties: dimensions of the device, hole dimensions and positions, microfluidic channel depth and width and surface roughness in the microfluidic channels are monitored and/or measured during and after processing.

Table 3 – Properties and their characterisation for glass types.

Material property	Reference standard or Semiconductor Equipment and Materials International (SEMI) standard	Measured value/s		
		D236® T eco	D236® bio	MEMpax®
Thickness tolerance	SEMI MF 1530 GBIR	$\pm \dots \mu\text{m}^*$		
Total thickness variation (TTV)	SEMI MF 1530 GBIR	$\leq \dots \mu\text{m}^*$		
Flatness	SEMI M1 GBINFER	$\leq \dots \mu\text{m}^*$		
Coefficient of thermal expansion (CTE)	Length measurements at different temperatures, ISO 7991 for glass	7.20 [$\mu\text{m}/\text{K}$]	7.20 [$\mu\text{m}/\text{K}$]	3.26 [$\mu\text{m}/\text{K}$]

**Depends on substrate thickness*

The channels in glass are isotropically wet etched with hydrofluoric acid-based etching solutions. Monitoring the dimensions of the width and depth of the microfluidic channels is crucial for microfluidic applications. The roughness of the channel plays an important role in the flow behaviour and should be as smooth as possible. The functionalisation of surfaces is used for biosensing applications and is also strongly influenced by the roughness (and wettability) of the surface.

Surface roughness measurements are presented in Deliverable 5 (D5) of this project ([link](#)).

Table 4 – Dimensional measured quantities and their characterisation relevant during and after processing of glass substrates used for microfluidic components.

Dimensional measured quantities in/on glass microfluidic components	Method	Measured value
Channel dimensions like depth or width	Optical microscope; white light interferometer, confocal laser microscopy, profilometer	Dimension [μm]
Dimensions of coating structures	Optical microscope; white light interferometer, confocal laser microscopy, profilometer	Dimension [μm]
Surface roughness of the channel, coating or device surface	AFM, white light interferometer, confocal laser microscopy; ISO 4287; ISO 21920 (new, draft)	R_a value [nm] = arithmetic mean height

5 Example protocols for measuring the dimensional characteristics of transfer standards

5.1 Glass transfer standards

As part of the A2.4.2 report, batches of transfer standards were designed and manufactured from two different materials (polymer and glass) with different internal dimensions and different designs. These transfer standards served as transfer standards in various work packages, tasks and activities in the MFMET project.

The protocol for measuring the dimensional characteristics of the transfer standards using a microscope is shown in the following section using the glass chip designs produced.

The glass transfer standards used in the project are microfluidic devices consisting of one or more main channels. Some of these are connected to one or more leakage channels.

The batch of glass transfer standards to be measured by optical microscopy consists of 8 different designs. For each design, 3 series have been produced, except for designs 6 & 7 (2 series) and 8 (1 series only).

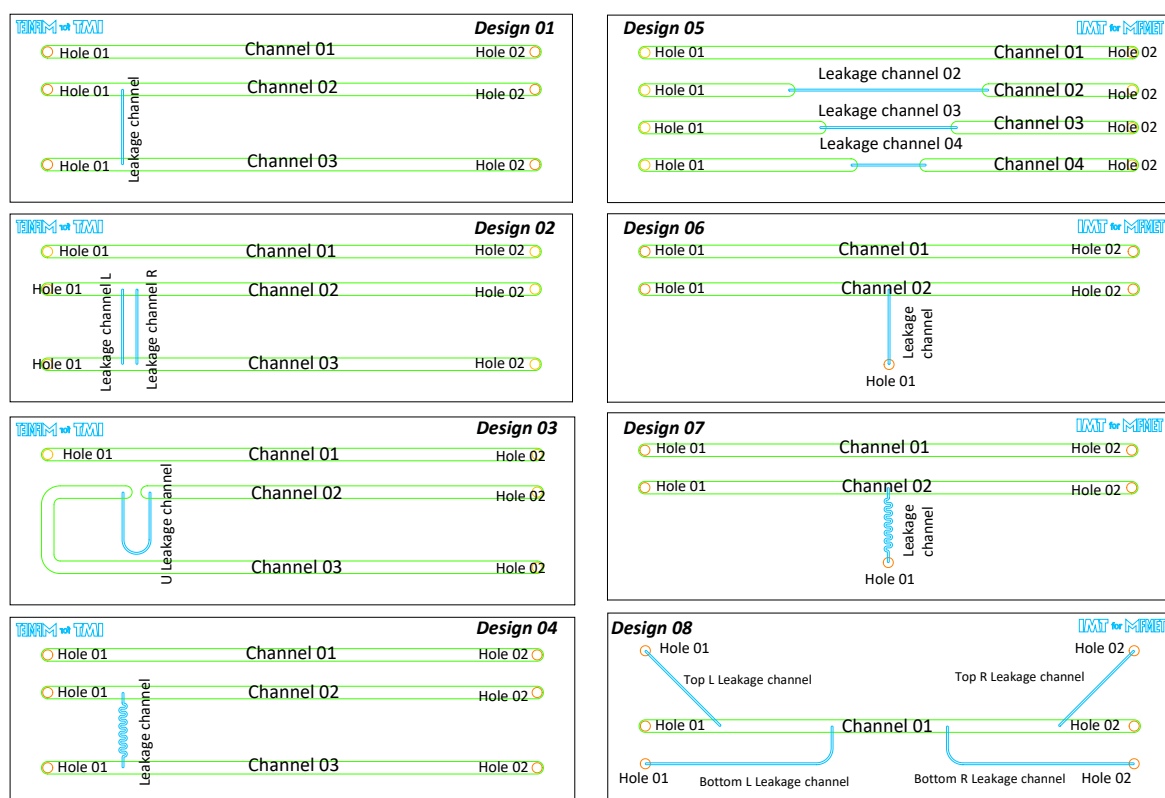


Figure 1 – Different designs of the 8 reference standards with the identification of each pattern to be measured.

5.2 Instruments

Two microscopes (Figure 2) were used depending on the dimensional range of the microfluidic components to be measured. Table 5 gives details of these two instruments, including the reference structures (see Figure 3) involved in the calibration process. Different reference structures/scales (test

patterns) allowed the instrument to be calibrated. This ensures that measurement results are traceable to SI units. The uncertainties associated with calibration are given in Table 5.

Table 5 – Information about the optical microscope and the stereo binocular microscope used for dimensional measurements.

Instrument	Reference	Range	Lens	Calibration	Uncertainty $U(k=2)$ linked to calibration
Digital Camera	Nikon D5300	> 10 000 μm	105 mm Macro lens	Scale bar	0.45%
Stereo microscope	Leica M165C	<10 000 μm	5x zoom	Scale Bar	0.27%
Optical microscope	Zeiss AXIO imager	<10 000 μm	X 2.5	Scale Bar	0.15%
Optical Microscope	Olympus BX53M	< 10 000 μm	X 1.5 X 5 X 15	Test pattern (Figure 3a)	0.1 %
Stereo Binocular Microscope	Leica wild M3Z	> 10 000 μm	X 2.56	Test pattern (Figure 3b)	2.0 %

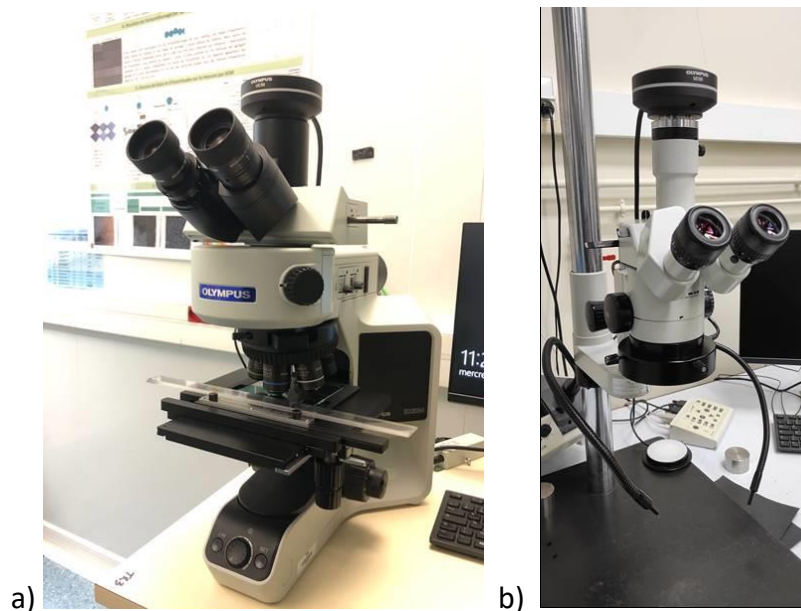


Figure 2 – a) Optical Microscope Olympus used for measuring width and hole diameters of the channel and leakage channel; b) Stereo Binocular Microscope Leica for the channel length measurements.

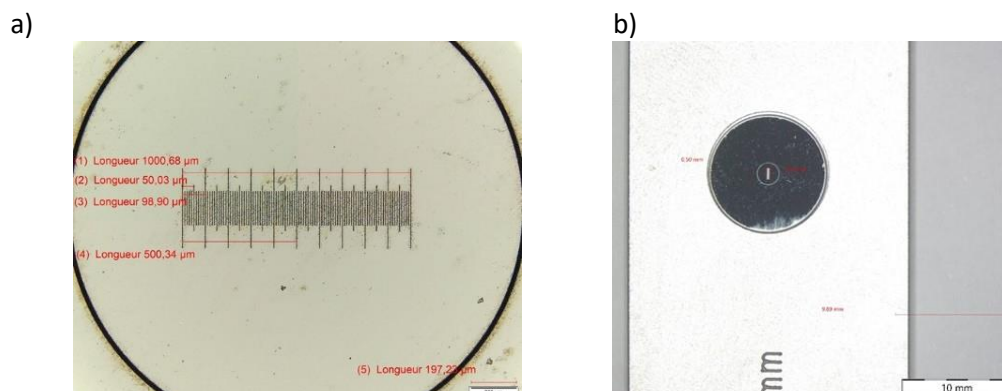


Figure 3 – Standards used for the calibration process: a) calibration test scale for Olympus BX53M and b) calibration test pattern for stereo binocular Leica.

5.3 Measurements procedure using a binocular microscope

The objective of this protocol is to determine the following dimensional parameters of the glass transfer standards described above:

- The width and length of the main and leakage channels.
- The diameter of the holes located at the ends of each main channel or leakage channel used as connectors.

Most of channels are linear but designs 3, 4, 7 and 8 present channels with curves (U, L or more complex shapes). Specific analysis tools were used to measure these non-linear channels.

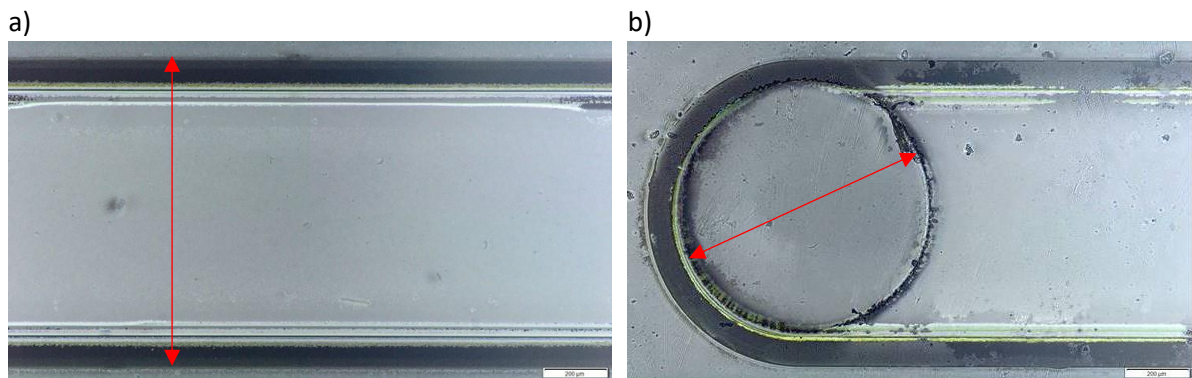
All tested designs are reported in Figure 3 with the various microfluidic components to be characterized.

The width of main and leakage channels, the length of leakage channels and the diameters of the hole for connection have been measured with Olympus microscope (X10 or X5). Images were analysed with the software Olympus Stream Essentials 2.3.3 (build 17023). This software includes a special function capable of merging all the focal planes into a single image. This tool allows us to identify the main focal plan on all images as shown in the Figure 4. The largest dimension was taken to be the width of the channels (red arrows). Regarding the hole measurement, a specific tool with circular shape was used. In this case, the main focal plan is quite difficult to identify. A large number of very close focal planes are observed. This is probably due to the hole-drilling phase during the manufacturing process of microfluidic devices.

Each measurement is repeated three times at different points in the channels and holes. A standard deviation, σ_r , is then calculated and represents both the repeatability of the measurement and the inhomogeneity of the patterns. Each measurement is associated with a comparison standard deviation σ which is equal to a standard uncertainty u calculated as the following quadratic sum:

$$u = \sigma = \sqrt{\sigma_r^2 + \sigma_c^2}$$

σ_c denotes the uncertainty linked to calibration.



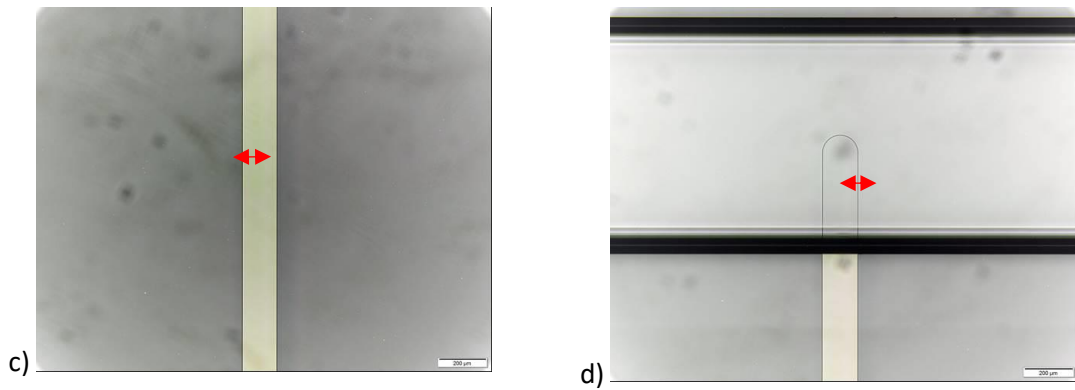


Figure 4 – Example of images obtained after merging and highlighting the main focal plans. A) middle of the channel 2; b) hole 2 of the channel 3; c) middle of the leakage channel and d) end of the leakage channel.

The length of non-linear channels (main or leakage) was measured with using specific tools available on the package Mountains Map version 10, software developed by Digital Surf. Depending on the complexity of the channel shape, the tools “distance between two points” and “customised path” were used (Figure 5). In both case, length was determined by following the median line of the channel width.

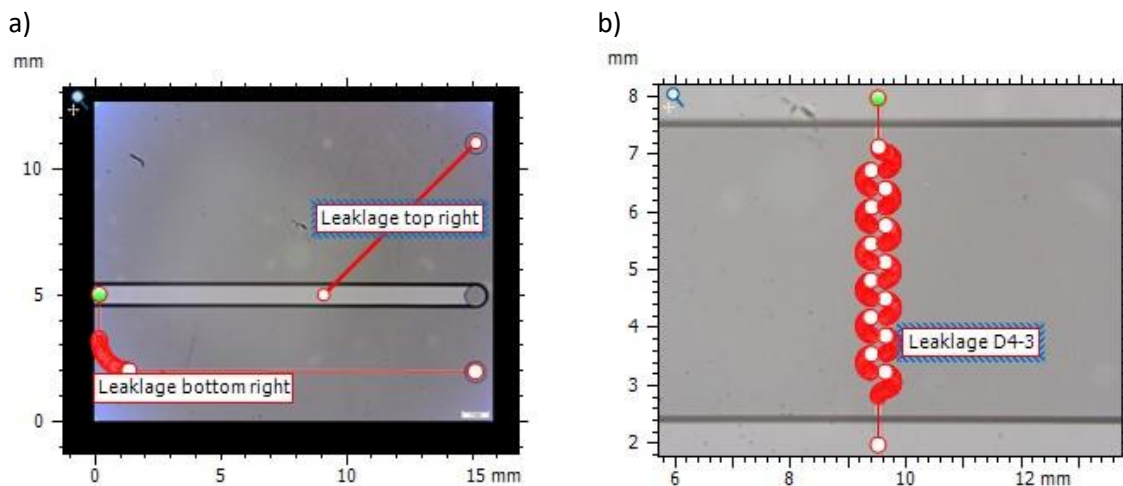


Figure 5 – Examples of how to use the tools “distance between two points” and “customised path” on a) leakage bottom right and top right of the design 8 and b) the leakage of the design 4.

The measured results are similar to those expected from the technical drawings.

All measurements are presented in ANNEX (Appendix) 1.

5.4 Image tiling to measure a whole device

While a typical microfluidic channel has a width of about 100s μm , the length of a microfluidic device is often in the order of a few centimetres. In this section, we presented the methods to measure an entire device via tiled images. The width and length of microfluidic channels of the glass transfer standards described above were measured.

Three instruments with a wide field of view were used, including 1) Leica M165C stereo microscope fitted with a Jenoptik PROGRES Speed XT Core3 camera (working distance 60 mm), 2) a Nikon D5300 camera fitted with a 105 mm, 1x, f/2.8 Macro lens, and 3) a Zeiss AXIO imager Z stand with a Ludl Biopoint2 motorised stage, 2.5x Plan Neofluar 0.085 numerical aperture (NA) Objective and Zeiss HRc camera. Calibration of these instruments were carried out using a standard reference bar (similar to these presented in Figure 3) to calibrate $\mu\text{m}/\text{pixel}$ and the uncertainty of the systems (see Table 5).

5.4.1 Procedure of tiling.

The total number of frames for covering the entire microfluidic channels depend on the field of view of the instrument. The accuracy of the measurement is affected by how the frames are stitched together, the quality of images and the precision of the instrument. Examples of using three instruments are described below (Figure 6).

For manually positioned samples, as in the case of Nikon D5300 camera and Leica M165C stereo microscope and, consecutive frames should take overlapped areas to facilitate subsequent tiling. Images can be stitched together in ImageJ by overlaying blemishes in successive frames, as illustrated in Figure 6.

For Nikon D5300 camera with large field of view, only two frames are needed to cover the whole main channel. The uncertainty of overlaying is ± 3 pixels/frame (1 pixel = 8.44 μm). However, the image quality is poor, meaning there is significant uncertainty in defining the end points of the channels. This is approximately 6 pixels at each end, so in total the error is of ± 15 pixels, which equals 0.31% of the total length of 40 mm. Furthermore, the leakage channels were not sufficiently visible in the images to warrant reliable measurements. Together with the uncertainty linked with the instrument (0.45% see Table 5), the potential uncertainty for this system is 0.76%, which is acceptable for a 40 mm length measurement.

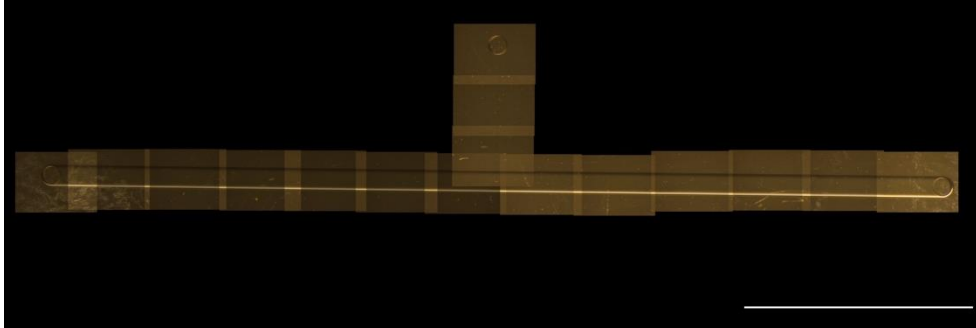
For Leica M165C stereo microscope, 13 frames are needed to cover the 40 mm length of the main channel. The uncertainty of overlaying is ± 3 pixels/frame (1 pixel = 1.72 μm), which give rise to a cumulative error of ± 36 pixels. This uncertainty is combined with the edge detection error (3 pixel at each end), resulting in around 0.18% uncertainty linked to the overlay images. Together with the uncertainty of the instrument (0.27%, see Table 5), this gives a total uncertainty of 0.45% for the total length of 40 mm measurement.

Zeiss AXIO imager contains a motorised Ludl Biopoint2 stage. Again, stitching to create a composite image could be achieved by overlaying blemishes in adjacent image frames, but the precision and reproducibility of the Ludl Biopoint2 stage (<1 μm) was sufficiently good that the results were indistinguishable. The notable advantage of this instrument was the higher NA of the 2.5x objective (NA=0.085), which gave images of better clarity, making definition of the channel and hole borders much clearer with the resulting improvement in the precision of the measurements. Therefore, the uncertainty in defining the end points is negligible (or at most at 1 pixel). So, the total uncertainty of the measurement is mainly associated with the instrument (0.15%, see Table 5).

In summary, the error in each measurement is determined by the precision at which it's possible to define the boundary of the channel in the camera image, which in turn is defined by the optical quality

(contrast and focus) of the image - the Zeiss objective has the best combination of NA (0.085) and sensor pixel spacing ($6.45\text{ }\mu\text{m}$) and so gives the best images. The Nikon D5300 has an NA of 0.18, but effective pixel spacing of $11.76\text{ }\mu\text{m}$ and the Leica has an NA of 0.03 and pixel size of $3.45\text{ }\mu\text{m}$.

(a)



(b)



(c)

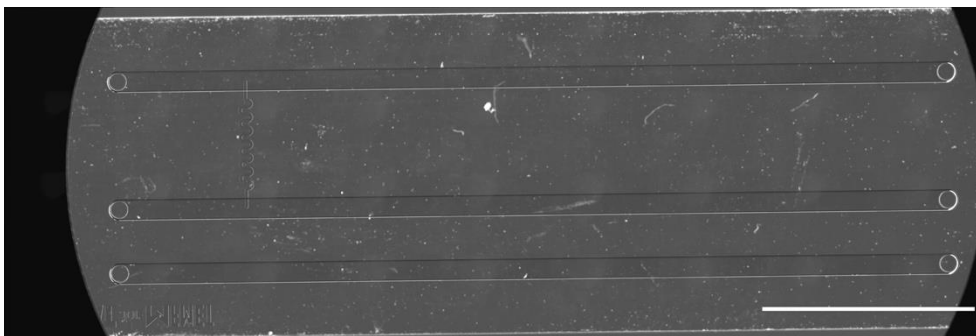


Figure 6 – Examples of stitching images together to measure the whole device. a) A stitched image for design 6 using Leica M165C stereo microscope. (b) A stitched image for design 1 using Nikon D5300 camera. (c) A stitched image for design 4 using Zeiss AXIO imager contains a motorised Ludl Biopoint2 stage. All scale bars are 10 mm.

5.5 Height measurements using confocal microscopy

Confocal microscopy is a fluorescence imaging technique. It operates in a confocal principle, which eliminates out-of-focus light from the focal planes (called optical sections) and collect serial optical sections. In comparison to conventional epifluorescence microscopy, confocal microscopy can produce three-dimensional images by stacking-up a series of z-images. As a non-invasive method,

confocal microscopy is well-suited to measure depth of an enclosed microfluidic channel. The resolution in z axis depends on the NA of objective lens.

Figure 7 and Figure 8 show a main channel of a polymer standard chip measured using two objective lenses: 1) 20x, NA=0.5 and 2) 100x, NA=1.3. The higher NA objective lens enables thinner optical slicing with optimal z-profile confocal slices being collected using z-step increments of 0.44 μm for the 100x 1.3 NA objective and 2.07 μm for the 20x 0.5 NA one. However, with the higher magnification and higher NA objective, for optical slices further away from the base of the channel, the fluorescence intensity significantly decreases due to the fluorophore solution this is nearer to the base of the channel absorbing both the laser light before it reaches the more distant slices the emitted fluorescence photons from the distant slice (fluorescence self-absorption). Note, in a confocal system, although the fluorescence light detected is confocal (i.e. selected by passing through a pinhole), the illumination light is not, and so the intensity of the illumination at particular z-heights is determined by the depth of field of the objective (for the 20x 0.5 NA, this is much greater than for the 100x, 1.3 NA)

This self-absorption can be seen clearly in the graphs of Figure 9 where the fluorescence intensity measured at the centreline of the channel (in the x-direction, perpendicular to both the long channel axis and the channel height axis) is plotted for successive slices. This data corresponds to a plot of the Integrated fluorescence counts of Figure 7 and Figure 8 vs. slice number, where the integrated fluorescence counts are those found at an image x-cut position 75 μm (20x) or 45 μm (100x), i.e. the centreline of the channel.

To make a measurement of the channel height using z-slice confocal measurements, first it is necessary to determine the slices at which the fluorescence intensity in the channel is significant. This can be done by comparing the image intensity to that measured outside of the channel (red lines, Figure 9). Secondly a decision needs to be made about the minimum value of fluorescence intensity within a confocal slice corresponds to that confocal slice being substantially within the channel. This decision is necessary because the confocality is not perfect i.e. for all practical pinhole sizes light from a range of z-distances will pass through it. For a homogeneous fluorescence solution such as is used here, a lower limit for fluorescence coming from a z-slice that is substantially within the channel could be taken as 1% of that found at the channel's mid-height (lower values could be used too, but this would require more careful consideration of the z-axis Airy profile for the pinhole and objective settings used).

Using this 1% criteria, it is possible to estimate that 37 of the 20x confocal slices are substantially within the channel, and using the z-axis step size of 2.07 μm (calibrated to be accurate to 0.1 μm using an internal encoder), the channel height of the device from the microfluidic ChipShop is estimated at $74.5 \pm 4 \mu\text{m}$ (there will be at least one slice uncertainty at both the top and bottom of the channel).

For the 100x confocal slices there are 166 slices above the 1% fluorescence intensity criteria, corresponding to a channel height estimate of $73.0 \pm 0.8 \mu\text{m}$.

Thus, the above both the 20x and 100x measurements are consistent with each other, with the 100x measurements having greater precision. However, importantly, although the images and plot profiles collected using the 100x objective shown in Figure 8 appear noisy (especially at distances further from the channel base), it is possible to make more accurate estimates of which slices have a fluorescence intensity above the designated 1% threshold.

In conclusion, the 100x objective provides better resolution and accuracy compared to the 20x (1% vs. 5%) for channels of 50 μm or above, it requires a longer time and the 100x accuracy would be closer

to 20% if the channel height was only 2 μm (smaller pinholes and smaller z-step sizes could be used, but it would be difficult to get below 5% accuracy for a 2 μm confocal fluorescence measurement).

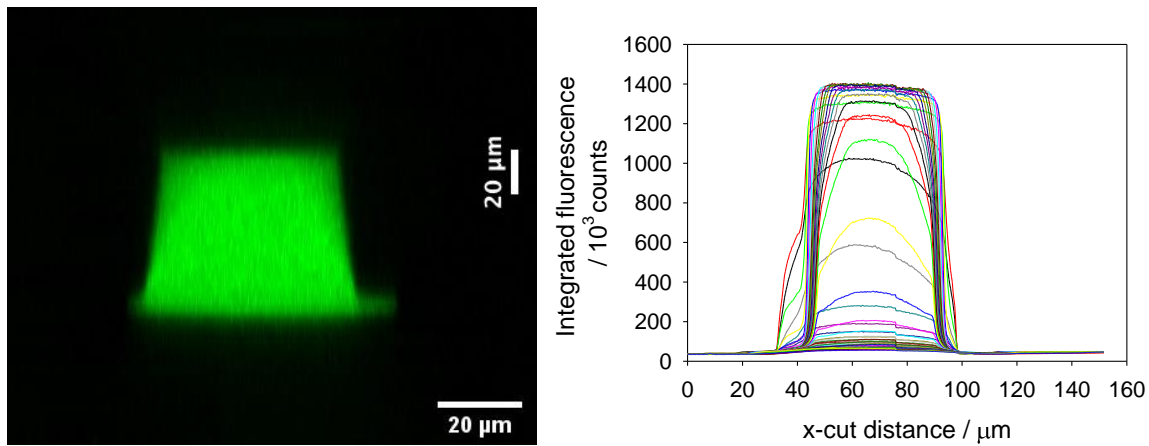


Figure 7 – Integrated fluorescence intensity from z-stack of 50 confocal slices (20x). Left: cross-section of channel height. Right image: intensity profile of z-series images. Each optical section (i.e. z-step) was set for 2.07 μm .

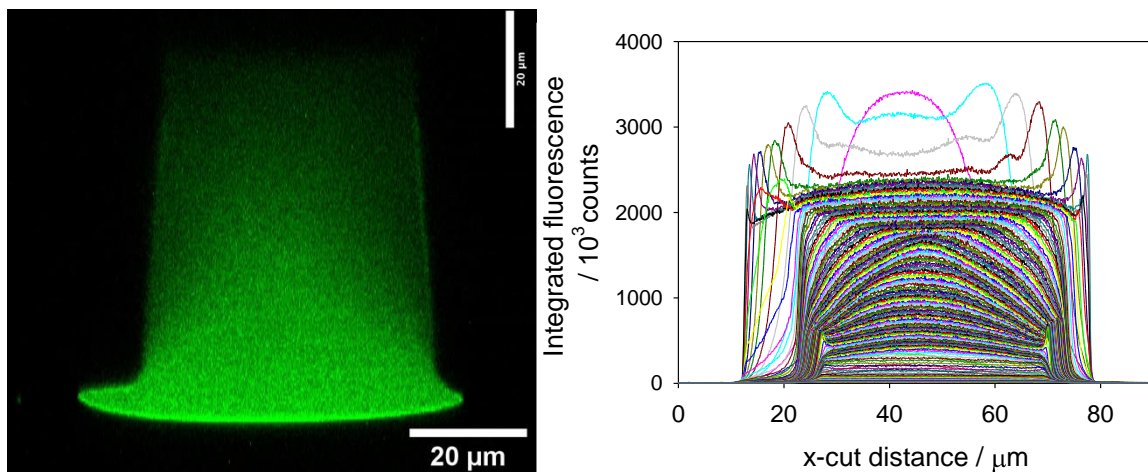


Figure 8 – Integrated fluorescence intensity from z-stack of 180 confocal slices (100x). Left: cross-section of channel height. Right image: intensity profile of z-series images. Each slice was set for 0.44 μm .

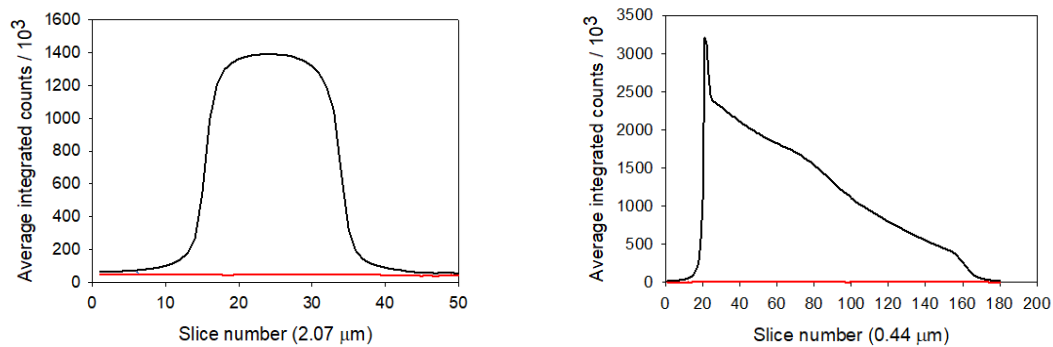


Figure 9 – Average fluorescence intensity for successive z slices measured in the centre of the channel (black) and to the side of the channel (red). Left: 20x objective, 2.07 μm slices; Right: 100x objective, 0.44 μm slices.

5.6 Measurements procedure using an optical profilometer

Optical profilometry is a method that uses light instead of a physical probe to characterise geometries. This allows non-destructive measurements without the need for direct contact with the object. Because of its light-based nature, it is particularly suitable for measurements within transparent substrates.

An OGP SmartScope ZIP250 with associated software was used to perform the measurements of the internal geometries. The measurement setup is shown in Figure 10.



Figure 10 – Optical profilometer OGP SmartScope ZIP250.

The instrument is recalibrated annually by OGP itself, which guarantees the accuracy shown in Table 6. OGP meets the requirements for ISO/IEC 17025-2017 (General Requirements for the Competence of Testing and Calibration Laboratories). It is important to note the difference in uncertainty between measurements where the stage has moved a distance L between two measurement points and static in-image measurements.

Table 6 – Information about the optical profilometer used for dimensional measurements.

Instrument	Reference	Range	Lens	Calibration	Uncertainty $U(k=2)$ linked to calibration
Optical Profilometer	OGP SmartScope ZIP250	$> 5 \mu\text{m}$	X 1 X 2	Annual calibration by the manufacturer OGP	In plane (XY): $\pm 2 \mu\text{m} + 4L/1000$ Vertically (Z): $\pm 2.5 \mu\text{m} + 5L/1000$ In-image: $< 1 \mu\text{m}$

The OGP SmartScope ZIP250 can automatically focus on a focal plane within an initially user-defined margin. The software then directly processes this image to identify geometric features, which are then used to measure the dimension of interest.

In practice, to determine a channel width (main or leakage), the profilometer should find the focus plane at the top of the channel, identify the outermost edges and then measure the width between these edges.

The depths of all channels were measured by determining a focus plane at the top and bottom of the channel using the “Focus” software tool to establish a point in 3D space on each plane. The software then measured the distance in Z between these two points to determine the channel depth.

The length of the main channels was taken as the maximum distance between the inlet and outlet holes. The hole diameter was determined using the “FeatureFinder” software tool set to determine a circle.

Difficulties arose in measuring the lengths of the more complex non-linear (non-straight) channels. Attempts were made to measure the lengths of the L, U and S shaped channels with many different settings. However, no reproducible parameters could be found.

The steps described above are programmable on the OGP SmartScope ZIP250. This means that a specific measurement protocol with positions, fields of view, focus zones, illumination and image processing settings can be stored in a programme, allowing repeatable tests on identical objects. A measurement programme created once is then run three times on each chip.

An average and standard deviation (σ_r) were determined from the data of each of these runs. Together with the uncertainty associated with the calibration of the instrument (σ_c), an overall measurement uncertainty (u) is calculated using the following formula:

$$u = \sqrt{\sigma_c^2 + \sigma_r^2}$$

5.7 Conclusions

A well define protocol is fundamental to perform accurate dimensional measurements of microfluidic components. In this report information on several method and reference standards used depending on the quantity to measured are indicated. Also, a protocol of dimension depth and with measurements in microfluidic channels is explained and detail and numerical examples are provided.

6 References

- [1] A.W. Martinez, S.T. Phillips, E. Carrilho, S.W. Thomas, H. Sindi, and G.M. Whitesides. *Simple Telemedicine for Developing Regions: Camera Phones and Paper-Based Microfluidic Devices for Real-Time, Off-Site Diagnosis*. Anal Chem. 2008, 80(10): 3699–3707.
- [2] Wang, B., Li, Y., Zhou, M. et al. Smartphone-based platforms implementing microfluidic detection with image-based artificial intelligence. Nat Commun 14, 1341 (2023). <https://doi.org/10.1038/s41467-023-36017-x>.
- [3] J. Howell, T.C. Hammarton, Y. Altmann and M. Jimenez, High-speed particle detection and tracking in microfluidic devices using event-based sensing, Lab Chip, 2020, 20, 3024.

ANNEX (Appendix) 1

Results obtained on Glass Chips with the instruments described in section 5.2.

Results obtained with the Optical Microscope Olympus BX53M and the Stereo Binocular Microscope Leica wild M3Z.

The data in the yellow boxes correspond to measurements taken with the binocular microscope.

Measurement results obtained on the three series of the design 01:

Design01 - serie 01	Hole 01		Hole 02		width		Length	
	Diam.	σ	Diam.	σ	Meas.	σ	Meas.	σ
Channel 01	813,14	11,37	829,02	1,61	998,10	1,78	40121,78	802
Channel 02	822,85	3,55	821,10	0,82	1001,59	2,93	40136,43	803
Channel 03	822,20	3,93	825,52	0,17	999,26	1,35	40078,11	802
Leakage Channel					152,60	0,35	6002,60	6

Design01 - serie 02	Hole 01		Hole 02		width		Length	
	Diam.	σ	Diam.	σ	Meas.	σ	Meas.	σ
Channel 01	802,07	9,27	812,18	7,70	1003,47	1,44	39786,32	796
Channel 02	805,23	9,44	805,64	4,38	1003,62	3,08	39786,50	796
Channel 03	804,25	14,37	810,86	1,41	1004,21	3,24	39771,98	795
Leakage Channel					153,02	4,07	6002,60	6

Design01 - serie 03	Hole 01		Hole 02		width		Length	
	Diam.	σ	Diam.	σ	Meas.	σ	Meas.	σ
Channel 01	820,95	3,51	826,10	7,96	997,38	0,89	39289,01	786
Channel 02	825,36	1,18	820,13	9,68	999,72	5,49	39289,04	786
Channel 03	819,14	2,10	822,47	5,12	997,58	0,89	39289,12	786
Leakage Channel					153,40	1,68	6002,60	6



Figure 11 – Technical drawing of design 01.

Measurement results obtained on the three series of the design 02:

Design02 - serie 01	Hole 01		Hole 02		width		Length	
	Diam.	σ	Diam.	σ	Meas.	σ	Meas.	σ
Channel 01	826,94	0,12	828,32	3,57	996,94	2,42	39877,08	798
Channel 02	822,42	2,98	831,55	12,83	1001,21	2,93	39865,55	797
Channel 03	819,50	16,05	821,95	3,05	997,33	3,07	39865,53	797
L Leakage Channel					152,06	0,67	6009,63	6
R Leakage Channel					152,06	0,67	6009,60	6

Design02 - serie 02	Hole 01		Hole 02		width		Length	
	Diam.	σ	Diam.	σ	Meas.	σ	Meas.	σ
Channel 01	815,46	7,49	821,41	4,67	997,00	0,89	39318,21	786
Channel 02	817,44	11,14	819,02	10,72	996,61	1,00	39303,58	786
Channel 03	823,39	17,58	820,22	13,39	997,39	1,69	39288,95	786
L Leakage Channel					153,01	2,10	6013,47	6
R Leakage Channel					153,40	2,20	6018,13	6

Design02 - serie 03	Hole 01		Hole 02		width		Length	
	Diam.	σ	Diam.	σ	Meas.	σ	Meas.	σ
Channel 01	810,74	6,54	823,15	4,71	1000,87	1,21	39464,45	789
Channel 02	814,65	5,85	821,57	4,59	1000,10	3,02	39405,93	788
Channel 03	818,38	9,65	810,08	14,19	1000,49	1,34	39391,55	788
L Leakage Channel					152,24	0,33	6018,14	6
R Leakage Channel					151,66	0,67	6022,82	6

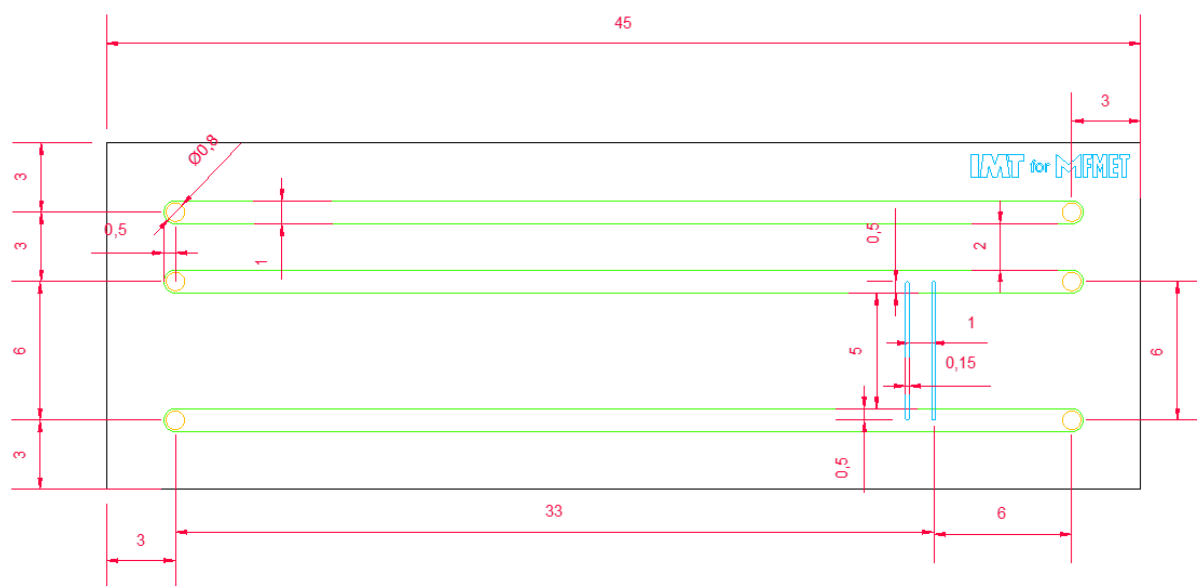


Figure 12 – Technical drawing of design 02.

Measurement results obtained on the three series of the design 03:

Design03 - serie 01	Hole 01		Hole 02		width		Length	
	Diam.	σ	Diam.	σ	Meas.	σ	Meas.	σ
Channel 01	829,00	9,03	817,92	17,12	999,42	1,24	39873,56	797
Channel 02			832,62	13,40	999,37	1,97	32056,72	641
Channel 03			832,62	11,11	996,94	1,34	50970,5	1019
U Leakage Channel					153,22	0,67	10949,00	219

Design03 - serie 02	Hole 01		Hole 02		width		Length	
	Diam.	σ	Diam.	σ	Meas.	σ	Meas.	σ
Channel 01	810,25	2,13	813,94	10,03	999,52	0,58	39669,10	793
Channel 02			824,56	2,91	1000,87	2,42	31881,34	638
Channel 03			819,08	19,24	996,59	1,34	50945,00	1019
U Leakage Channel					153,79	1,21	11003,00	220

Design03 - serie 03	Hole 01		Hole 02		width		Length	
	Diam.	σ	Diam.	σ	Meas.	σ	Meas.	σ
Channel 01	823,21	11,25	815,11	5,15	1000,49	0,67	39844,19	797
Channel 02			816,26	2,97	999,32	1,87	32012,73	640
Channel 03			813,60	0,83	1001,07	1,00	51075,00	1021
U Leakage Channel					151,07	0,34	10995,00	220

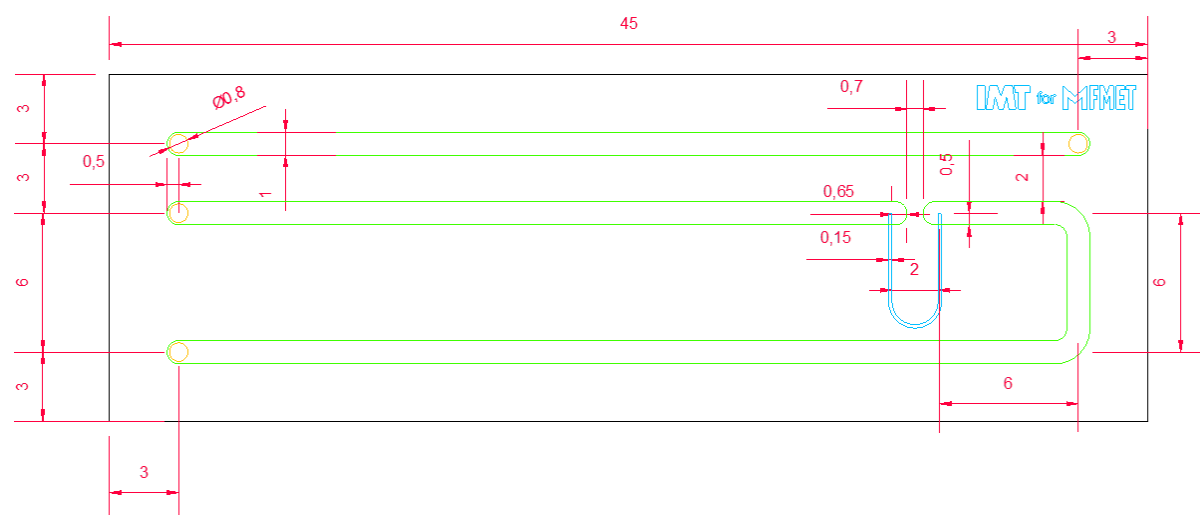


Figure 13 – Technical drawing of design 03.

Measurement results obtained on the three series of the design 04:

Design04 - serie 01	Hole 01		Hole 02		width		Length	
	Diam.	σ	Diam.	σ	Meas.	σ	Meas.	σ
Channel 01	808,13	12,46	805,34	29,77	999,64	1,19	39581,55	792
Channel 02	816,76	9,38	828,12	1,83	998,88	1,34	39581,70	792
Channel 03	815,57	6,41	821,38	5,80	999,66	2,34	39581,95	792
Leakage Channel					151,29	1,17	10852,00	217

Design04 - serie 02	Hole 01		Hole 02		width		Length	
	Diam.	σ	Diam.	σ	Meas.	σ	Meas.	σ
Channel 01	808,72	6,00	811,85	2,81	998,93	1,75	40078,16	802
Channel 02	812,47	2,33	814,20	0,23	998,94	0,59	40092,77	802
Channel 03	811,57	0,25	814,26	2,54	998,74	1,87	40093,07	802
Leakage Channel					150,88	0,89	10890,00	218

Design04 - serie 03	Hole 01		Hole 02		width		Length	
	Diam.	σ	Diam.	σ	Meas.	σ	Meas.	σ
Channel 01	812,39	1,97	812,34	0,40	999,32	1,21	39566,62	791
Channel 02	810,35	1,95	813,74	0,15	999,13	1,78	39566,65	791
Channel 03	810,66	3,36	813,91	0,40	999,71	1,78	39552,16	791
Leakage Channel					151,07	0,68	10980,00	220

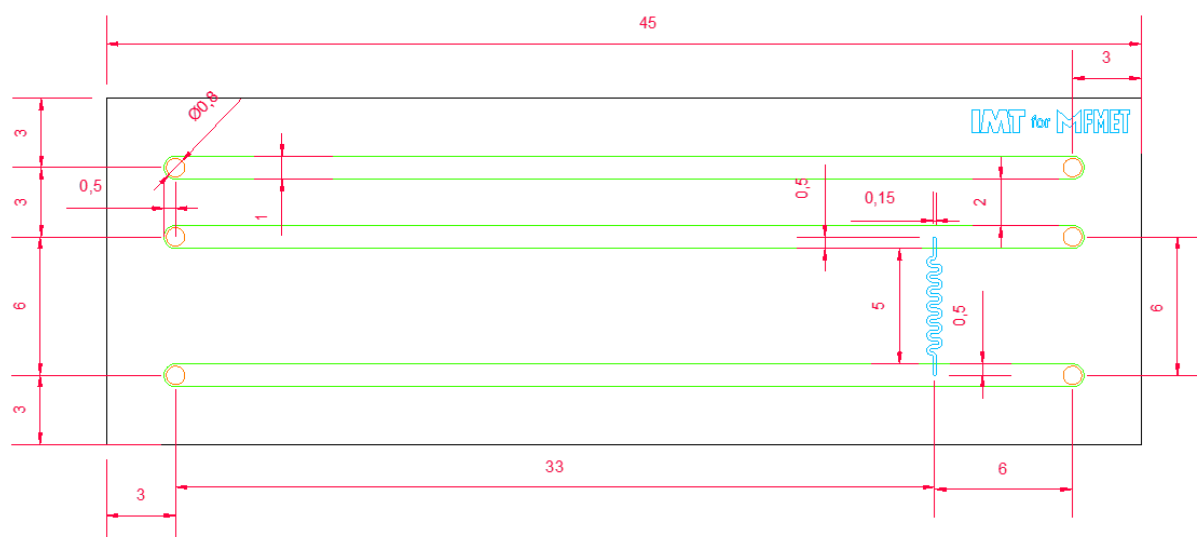


Figure 14 – Technical drawing of design 04.

Measurement results obtained on the three series of the design 05:

Design05 - serie 01		Hole 01		Hole 02		width		Length	
		Diam.	σ	Diam.	σ	Meas.	σ	Meas.	σ
Channel 01		813,64	15,92	802,89	13,84	996,94	2,68	39581,17	792
Channel 02		810,21	17,56	818,96	14,92	995,00	2,33	12258,62	245
								R 12404,73	248
Channel 03		818,54	9,81	812,46	19,75	997,32	4,20	14742,49	295
								R 14859,37	297
Channel 04		810,07	14,72	813,21	13,60	995,38	1,35	17270,19	345
								R 17328,64	347
Leakage Channel 02						153,23	2,42	16158,90	16
Leakage Channel 03						153,61	0,33	11053,48	11
Leakage Channel 04						152,45	2,43	6028,32	6

Design05 - serie 02		Hole 01		Hole 02		width		Length	
		Diam.	σ	Diam.	σ	Meas.	σ	Meas.	σ
Channel 01		813,99	6,07	812,51	3,97	997,77	2,10	39727,32	795
Channel 02		802,25	1,57	810,69	0,81	999,91	2,35	12317,14	246
								R 12448,56	249
Channel 03		807,11	1,67	812,54	3,27	999,13	1,35	14786,33	296
								R 14947,07	299
Channel 04		806,38	2,01	811,25	0,81	1000,31	2,38	17270,19	345
								R 17401,69	348
Leakage Channel 02						153,01	0,58	16123,50	16
Leakage Channel 03						152,04	0,33	11042,73	11
Leakage Channel 04						152,62	0,67	6008,82	6

Design05 serie 03		Hole 01		Hole 02		width		Length	
		Diam.	σ	Diam.	σ	Meas.	σ	Meas.	σ
Channel 01		811,24	1,29	813,17	2,48	997,42	1,49	39362,01	787
Channel 02		814,07	0,28	813,32	1,10	996,41	1,46	12258,63	245
								R 12331,71	247
Channel 03		812,81	1,25	812,83	0,81	997,77	3,54	14684,05	294
								R 14771,72	295
Channel 04		809,63	1,54	810,60	2,48	999,71	3,21	17094,86	342
								R 17240,99	345
Leakage Channel 02						151,07	0,68	16137,40	16
Leakage Channel 03						151,66	0,33	11051,98	11
Leakage Channel 04						151,07	0,68	6022,81	6

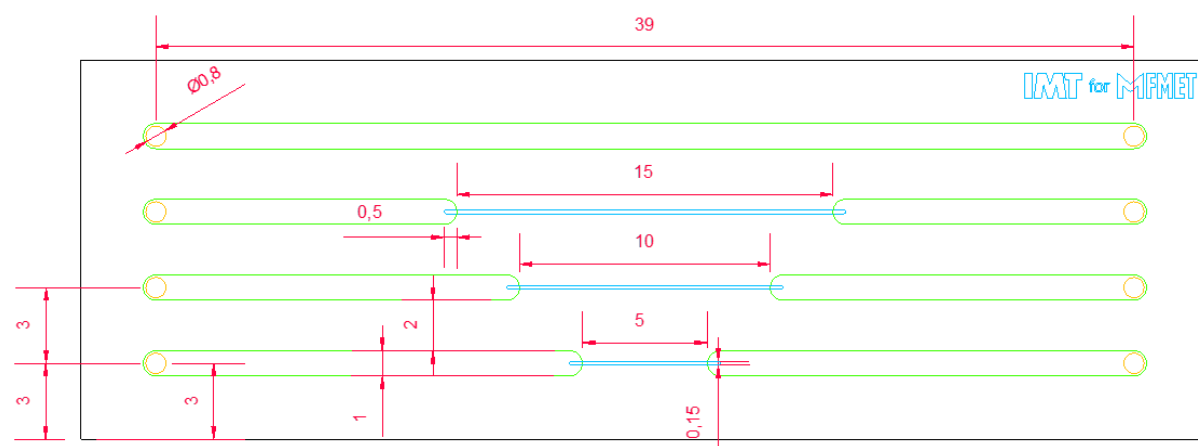


Figure 15 – Technical drawing of design 05.

Measurement results obtained on the three series of the design 06:

Design06 - serie 01	Hole 01		Hole 02		width		Length	
	Diam.	σ	Diam.	σ	Meas.	σ	Meas.	σ
Channel 01	798,04	6,98	822,18	9,62	995,83	2,05	39508,72	790
Channel 02	815,29	12,99	821,93	9,92	997,97	2,01	39508,89	790
Leakage Channel	812,46	1,98			151,85	0,67	6018,13	6

Design06 - serie 02	Hole 01		Hole 02		width		Length	
	Diam.	σ	Diam.	σ	Meas.	σ	Meas.	σ
Channel 01	814,95	0,81	816,33	3,37	996,30	0,90	39829,72	797
Channel 02	812,70	0,81	813,85	3,43	997,82	3,05	39829,68	797
Leakage Channel	810,82	1,26			150,88	1,21	6022,82	6

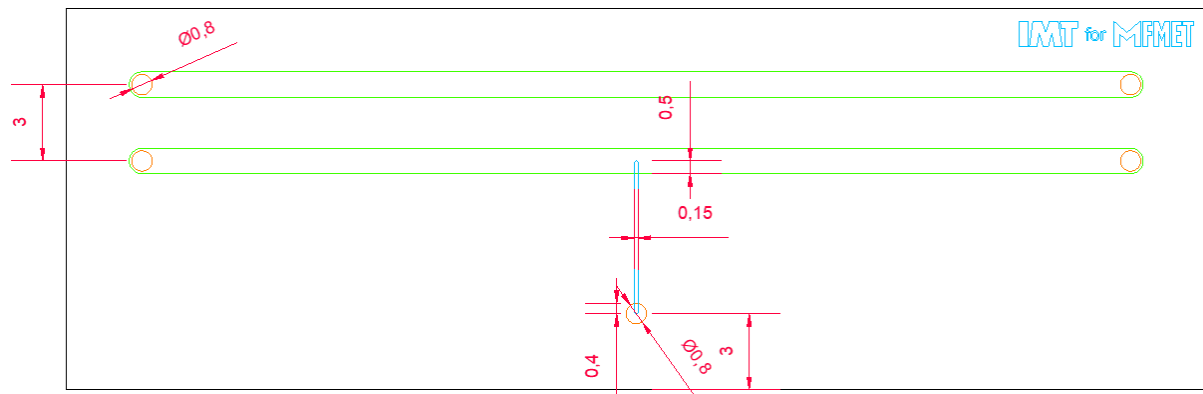


Figure 16 – Technical drawing of design 06.

Measurement results obtained on the three series of the design 07:

Design07 - serie 01	Hole 01		Hole 02		width		Length	
	Diam.	σ	Diam.	σ	Meas.	σ	Meas.	σ
Channel 01	811,56	10,63	822,37	5,11	996,80	1,21	40063,33	801
Channel 02	816,76	11,62	821,93	9,92	997,97	1,46	40077,95	802
Leakage Channel	820,53	6,88			151,85	1,16	10930,00	219

Design07 - serie 02	Hole 01		Hole 02		width		Length	
	Diam.	σ	Diam.	σ	Meas.	σ	Meas.	σ
Channel 01	812,75	3,54	813,54	1,60	996,50	2,73	39727,32	795
Channel 02	811,49	3,50	812,65	2,33	994,47	3,87	39742,02	795
Leakage Channel	810,59	1,75			151,46	0,89	10900,00	218

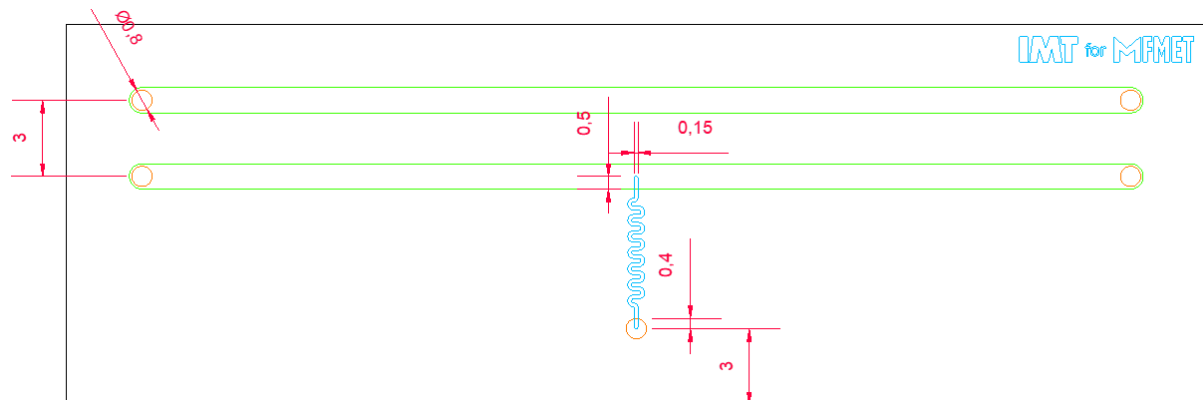


Figure 17 – Technical drawing of design 07 (length of leakage channel = 10 mm).

Measurement results obtained on the three series of the design 08:

Design08	Hole 01		Hole 02		width		Length	
	Diam.	σ	Diam.	σ	Meas.	σ	Meas.	σ
Channel 01	816,50	6,68	821,99	1,17	996,80	1,78	39741,89	795
Bottom L Leakage channel	825,30	3,71			153,01	0,58	17470	349
Bottom R Leakage	825,09	6,32			155,15	0,33	17460	349
Top L Leakage	819,58	12,12			152,49	1,19	8583,83	9
Top RLeakage	822,23	10,57			153,45	1,80	8540,75	9

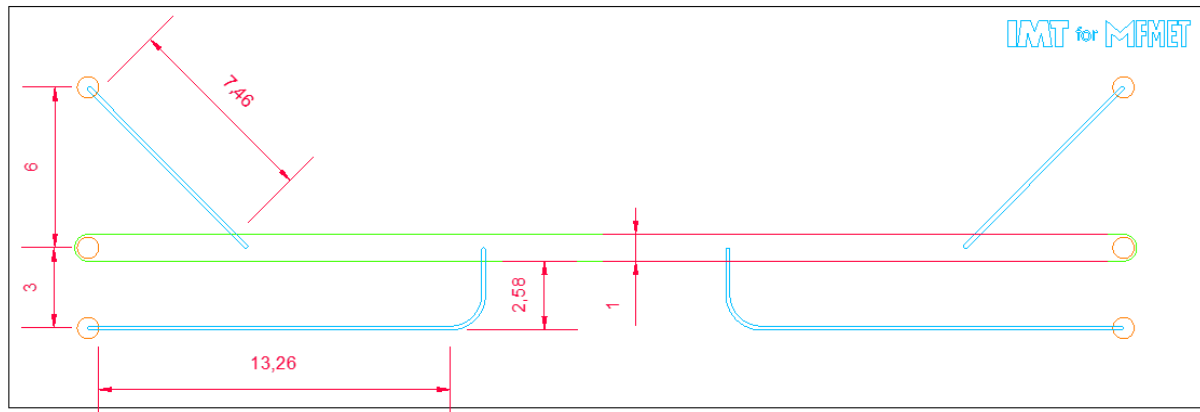


Figure 18 – Technical drawing of design 08.

Results obtained with (1) Digital Camera Nikon D5300; (2) Stereo microscope Leica M165C and (3) Optical microscope Zeiss AXIO imager, see also Figure 1.

Method (1) Nikon D5300 digital camera fitted with a 105 mm macro lens

- The resolution with this lens: 8.436 $\mu\text{m}/\text{pixel}$
- Uncertainty: 8 pixel from the end-to-end
- Uncertainty rate: 0.45%

Design 01 - series 01	Hole 01		Hole 02		Width		Depth		Length	
	Diam.	s	Diam.		Meas.	s	Meas.	s	Meas.	s
Channel 01	835.00		835.00		877.00		N/A	N/A	37 670.00	
Channel 02	869.00		844.00		869.00		N/A	N/A	37 689.00	
Leakage Channel	N/A				N/A		N/A	N/A		

Design 02 - series 01	Hole 01		Hole 02		Width		Depth		Length	
	Diam.	s	Diam.		Meas.	s	Meas.	s	Meas.	s
Channel 01	894.00		928.00		895.00		N/A	N/A	37 612.00	
Channel 02	793.00		936.00		877.00		N/A	N/A	37 646.00	
Leakage Channel	N/A				N/A		N/A	N/A		

Design 03 - series 01	Hole 01		Hole 02		Width		Depth		Length	
	Diam.	s	Diam.		Meas.	s	Meas.	s	Meas.	s
Channel 01	861.00		N/A		852.00		N/A	N/A	38 439.00	
Channel 02	886.00		N/A		852.00		N/A	N/A	30 312.00	
Section perpendicular to main channel 1	N/A		N/A		861.00				5 907.00	
Section leading into U-shaped leakage channel from perpendicular section above	N/a				894.00		N/A	N/A	5 873.00	

Design 04 - series 01	Hole 01		Hole 02		Width		Depth		Length	
	Diam.	s	Diam.		Meas.	s	Meas.	s	Meas.	s
Channel 01	827.00		801.00		835.00		N/A	N/A	37 620.00	
Channel 02	866.00		866.00		832.00		N/A	N/A	37 627.00	
Leakage Channel	N/a				N/A		N/A	N/A		

Design 05 - series 01	Hole 01		Hole 02		Width		Depth		Length	
	Diam.	s	Diam.		Meas.	s	Meas.	s	Meas.	s
Channel 01	819.00				877.00				37 579.00	
L Channel 02	810.00		N/A		852.00		N/A	N/A	16 271.00	
R Channel 02	810.00		N/A		867.00		N/A	N/A	16 237.00	
L channel 03	852.00				894.00				13 730.00	
R Channel 03	753.00				928.00				13 775.00	
L channel 04	810.00				860.00				11 316.00	
R Channel 04	767.00		N/A		843.00				11 267.00	

Design 06 - series 02	Hole 01		Hole 02		Width		Depth		Length	
	Diam.	s	Diam.		Meas.	s	Meas.	s	Meas.	s
Channel 01	805.00		852.00		856.00		N/A	N/A	37 713.00	
Channel 02	N/A		N/A		N/A		N/A	N/A	N/A	
Leakage Channel	779.00				N/A		N/A	N/A	5081	

Design 07 - series 01	Hole 01		Hole 02		Width		Depth		Length	
	Diam.	s	Diam.		Meas.	s	Meas.	s	Meas.	s
Channel 01	860.00		844.00		843.00		N/A	N/A	37 559.00	
Channel 02	N/A		N/A		N/A		N/A	N/A	N/A	
Leakage Channel			804		N/A		N/A	N/A	5081	

Design 06 - series 02	Hole 01		Hole 02		Width		Depth		Length	
	Diam.	s	Diam.		Meas.	s	Meas.	s	Meas.	s
Channel 01	810.00		782.00		894.00		N/A	N/A	37 779.00	
Channel 02	N/A		N/A		N/A		N/A	N/A	N/A	
Leakage Channel	/				N/A		N/A	N/A	/	

Method (2) Zeiss AXIO imager 2.5x objective optical microscope

- The resolution with this lens: 3.749 $\mu\text{m}/\text{pixel}$
- Uncertainty: 1 pixel from the end-to-end
- Uncertainty rate: 0.15%

Design 01 - series 01	Hole 01			Hole 02			Width			Depth		Length	
	Diam.	s		Diam.			Meas.	s		Meas.	s	Meas.	s
Channel 01	829.00		#DIV/0!	829.00		#DIV/0!	986.00		#DIV/0!	N/A	N/A	38 171.00	
Channel 02	829.00		#DIV/0!	829.00		#DIV/0!	986.00		#DIV/0!	N/A	N/A	38 128.00	
Leakage Channel	N/A		#DIV/0!				147.00		#DIV/0!	N/A	N/A	5 034.00	

Design 02 - series 01	Hole 01			Hole 02			Width			Depth		Length	
	Diam.	s		Diam.			Meas.	s		Meas.	s	Meas.	s
Channel 01	826.00		#DIV/0!	834.00		#DIV/0!	982.00		#DIV/0!	N/A	N/A	38 235.00	
Channel 02	884.00		#DIV/0!	865.00		#DIV/0!	982.00		#DIV/0!	N/A	N/A	38 227.00	
L Leakage Channel							152.00					5 052.00	
R Leakage Channel	N/A		#DIV/0!				148.00		#DIV/0!	N/A	N/A	5 052.00	

Design 04 - series 01	Hole 01			Hole 02			Width			Depth		Length	
	Diam.	s		Diam.			Meas.	s		Meas.	s	Meas.	s
Channel 01	828.00		#DIV/0!	836.00		#DIV/0!	986.00		#DIV/0!	N/A	N/A	38 133.00	
Channel 02	824.00		#DIV/0!	825.00		#DIV/0!	986.00		#DIV/0!	N/A	N/A	38 137.00	
Leakage Channel	N/A		#DIV/0!				N/A		#DIV/0!	N/A	N/A		

Method (3) Leica M165C stereo microscope

- The resolution with this lens: 1.720 $\mu\text{m}/\text{pixel}$
- Uncertainty: 4 pixel from the end-to-end
- Uncertainty rate: 0.275%

Design 06 - series	Hole 01			Hole 02			Width			Depth		Length	
	Diam.	s		Diam.			Meas.	s		Meas.	s	Meas.	s
Channel 01	816.00		#DIV/0!	808.00		#DIV/0!	969.00		#DIV/0!	N/A	N/A	38 079.00	
Leakage Channel	N/A		#DIV/0!	787			155.00		#DIV/0!	N/A	N/A	5 070.00	